Effect of Alloy Composition on the Oxidation Behaviour and Cr Evaporation of High-Cr Steels for SOFC Cathode Air Preheaters

Zhang, Kun; Hong, Jong-Eun; Steinberger-Wilckens, Robert

ISBN 978-3-905592-23-8

A0807 (Candidate: EFCF Special Issue Series, www.EFCF.com/LIB)

Effect of Alloy Composition on the Oxidation Behaviour and Cr Evaporation of High-Cr Steels for SOFC Cathode Air Preheaters

Kun Zhang (1), Jong-Eun Hong (2), Robert Steinberger-Wilckens (1)
(1) Fuel Cell Research Group, School of Chemical Engineering, University of Birmingham, B15 2TT, United Kingdom
(2) Fuel Cell Laboratory, Korea Insititute Research, 152 Gajeong-ro, Yuseong-gu, Daejeon, 34129, Republic of Korea
Tel.: +44 7544144694
kxz295@student.bham.ac.uk

Abstract

The Cathode Air Preheater (CAPH) acts as a heat exchanger, recovering heat from the exhaust gas to heat air before it enters the solid oxide fuel cell (SOFC) stacks. The state of art of the CAPH design employs an advanced alloy containing high content of Cr to offer improved oxidation resistance under isothermal and cyclic conditions and provide good high temperature strength. Nevertheless, in high-temperature (>600 °C) oxidising environments, the volatile Cr-rich species carried from the CAPH into the SOFC cathode component are a major source of cathode degradation that limits the lifetime of SOFC systems with metallic CAPH. For a more systematic approach, it is important to measure the oxidation rate and quantify the amount of evaporated Cr-species of a variety of stainless steel materials. This study compares the oxidation performance of the aluminium containing Aluchrom 318 alloy and the nickel based Inconel 625 alloy at high temperature. Furthermore, the oxidation behaviour of the uncoated stainless steel 309 is also compared with a PVD aluminised version of same material. The aim of this research is to investigate the Cr retention ability of the Al_2O_3-rich layer formed on the outer layer of aluminium-containing alloys.
The materials have been investigated with respect to Cr evaporation and oxidation rate. High temperature oxidation tests have been implemented both isothermal and discontinuously in a tubular furnace for 3000 hours at 850 °C. The Cr evaporation tests have been continuously performed by applying a denuder technique, which allows time-resolved and accurate quantification of Cr evaporation from alloys at high temperature. The chromium evaporation of uncoated SS309 was dramatically decreased by aluminising. The experiments showed that Cr retention of the aluminised SS309 is comparable to that of alumina-forming steel, AluChrom 318, over 168 hours. The formed oxide scales were studied by XRD and SEM/EDX. The surface SEM/EDX results indicated that the AluChrom 318 and aluminised SS309 appeared to be covered with an oxide layer containing a high amount of aluminium and oxygen. XRD analysis revealed that α-Al_2O_3 layer is formed for the Aluchrom 318 and the aluminised SS309. However, a large amount of spallation of Al_2O_3 scale was observed on the surface of the aluminised SS309, leading to the exposure of the Cr-rich oxide layer. The cross section SEM/EDX revealed that the α-Al_2O_3 layer formed on the Aluchrom 318 was continuous, and the thickness increased with exposure time.

ISBN 978-3-905592-23-8

1. Introduction

The residential SOFC system generally discharges a large amount of high temperature exhaust gas, which can be used for domestic hot water or space heating due to its high level of thermal energy. In addition, ceramic materials of a SOFC, such as cathode, anode, and electrolyte, are unable to resist steep temperature gradients [1]. Therefore, SOFCs need the cathode air to be pre-heated before it is introduced into the fuel cell systems. As air flow plays a function as coolant to sufficiently remove the heat produced inside the fuel cell system, its temperature and amount are important factors to the SOFC inlet and must be controlled. Therefore, thermal management in SOFC is especially significant for keeping the operating temperature under control and insuring both adequate feeding conditions for fuel and oxygen/air. The cathode air pre-heater (CAPH) is one of the most important balance of plant (BOP) components. The CAPH recovers the thermal energy from the exhaust gas to heat the air to target temperature (750 ˚C) before it enters into the fuel cell. The materials used for CAPH must be robust to ensure safe, reliable and continuous operation under the high working temperature. The project HEATSTACK is looking into issues of CAPH in SOFC systems, including manufacturability, structural integrity, and chromium release. The current CAPH prototype employs an advanced Cr-containing alloy to offer improved oxidation resistance under isothermal and cyclic conditions and provide sufficient mechanical strength.

However, high temperature oxidation and Cr vaporisation are still critical issues that will have detrimental effects on the SOFC stack. Volatilisation of hexavalent Cr such as CrO_3 and $CrO_2(OH)_2$ will form over the Cr_2O_3 scale in oxidising environment at high temperature [2-4]. A number of researchers have proven that $CrO_2(OH)_2$ is the dominant Cr-containing volatiles under SOFC cathode environment [4-6]. The evaporated chromium species that leaves the alloy surface eventually deposits onto and poisons the cathode, leading to significant performance degradation [7]. Taniguchi *et al.* [8] examined the deterioration of cell performance when alloy coupons were placed on the LSM cathode of the SOFC during cell tests. A decrease of cell voltage was already detected after 500 hours operation. The reduction of cell performance from 0.7 V to 0.1 V was due to the blockage of pores by Cr_2O_3, which decreased the number of active sites for the oxygen reduction reaction. Foremost among alloys for CAPH application are aluminium-containing materials, mainly because their excellent corrosion resistance is based on the protective alumina scales. Alumina-forming materials have been utilised for a wide range of applications such as catalyst supports in automotive application because of their high corrosion resistance and stability. Normally, the concentration of Cr inside alumina-forming alloys is around 20 wt.%. The added Cr boosts the formation of an external α-Al_2O_3 layer by reducing the ingress of oxygen into the alloy during high temperature exposure [9]. However, the ductility of alumina-forming alloys is considered to be poor due to their high Al content [10]. Another possible solution to the cathode-side chromate production is to form a protective alumina layer by surface aluminising. Aluminising enhances the oxidation resistance of alloys at high temperature without influencing the mechanical properties of the test materials in the core.

The purpose of this study was to quantitatively measure the Cr species evaporated from Inconel 625, AluChrom 318, uncoated SS309, and aluminised SS309 by means of the denuder technique at the temperature of 850 ˚C. This research also determined if the corrosion resistance and Cr evaporation performance of SS309 can be improved by aluminising. In addition, the suitability of aluminised chromia-forming alloys and alumina-forming alloys for CAPH application concerning the reduction of Cr evaporation will be discussed.

ISBN 978-3-905592-23-8

2. Materials and Methods

2.1 Materials

Three commercial alloys were selected for this research. The samples were coupons of the Cr-containing alloys with the dimensions 15×15×0.3 mm^3. The alloy compositions for these materials in wt.% are shown in Table 1. One material, stainless steel 309 (SS309), was additionally aluminised on both sides in order to compare the high temperature corrosion behaviour with uncoated SS309. The 1 µm aluminium film was coated by Teer Coating Ltd with a proprietary physical vapour deposition (PVD) process. All samples were exposed in an as-received status after being cleaned in acetone and ethanol using an ultrasonic bath.

Table 1: The chemical compositions of the researched materials supplied by manufacturer.

(wt.%)	Fe	Cr	Mn	Al	Ni	Si	Nb	W	Co	others
AluChrom 318	Bal.	18.8	0.21	3.58	0.24	0.32	0.73	2.02	--	Hf 0.06; Y 0.07 Zr 0.03; Cu 0.03 C 0.01; N 0.01
Inconel 625	5.0	20-23	0.5	0.4	Bal.	0.5	4.15	-	1.0	Ti 0.4; Mo 8-10 P 0.015; S 0.015
SS309	Bal.	22-24	2.0	--	12-15	0.75	--	--	--	C 0.2; P 0.045 S 0.03

2.2 Exposures

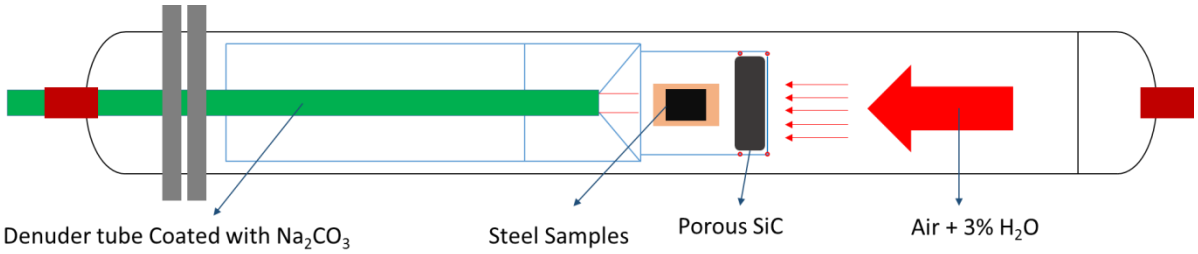

Figure 1. The schematic diagram of denuder technique.

For the Cr evaporation test, the volatile Cr species were measured by isothermally exposing three identical samples of stainless steel using a denuder technique [11] in a tubular furnace at 850 °C (Figure 1). The tests were carried out in an atmosphere consisting of air that was humidified with 3 vol% of water to simulate an SOFC cathode environment. The air flow rate was controlled to 6000 ml/min which corresponds to a regime where the evaporation rate is flow independent [11]. As shown in Figure 1, directly to upstream of the samples, a porous SiC functioning as a flow restrictor was placed obtain a uniform flow pattern. Downstream of the samples, the gas stream was fed through the quartz glass denuder tube, which had an i.d. of 5 mm. The inner wall of the denuder tube was coated with Na_2CO_3 which was used for Cr collection. The Cr-containing gas ($CrO_2(OH)_2$) produced in the simulated SOFC environment reacted with the Na_2CO_3 to produce Na_2CrO_4 on the basis of equation (1):

$$CrO_2(OH)_2\ (g) + Na_2CO_3\ (s) \rightarrow Na_2CrO_4\ (s) + H_2O\ (g) + CO_2\ (g) \quad (1)$$

After collection, the inside wall of the denuder tube was subsequently washed with 10 ml distilled water. UV-vis spectrophotometer analysis applied to the obtained solutions offered quantification of the total amount of evaporated Cr species.

ISBN 978-3-905592-23-8

A high temperature oxidation test was additionally carried out by exposing different types of materials simultaneously at the same temperature and flow for a total time of 2500 hours. The difference between the high temperature oxidation test and the Cr evaporation test was that in the former case stainless steel samples were removed at increasing time intervals for gravimetric measurement and characterisation. For Cr collection, the denuder tubes were replaced without cooling down the furnace, allowing for uninterrupted measurement of Cr evaporation.

2.3 Characterisation

The gravimetric measurements were carried out using a Cubis Micro Balance (MSA2.7S0TRDM). The microstructure of the surface of non-exposed and exposed samples were studied by scanning electron microscopy/energy dispersive X-ray spectroscopy (SEM/EDX) (Tabletop Microscope TM3030, Hitachi-Hitec)

3. Results

3.1 Mass Gain

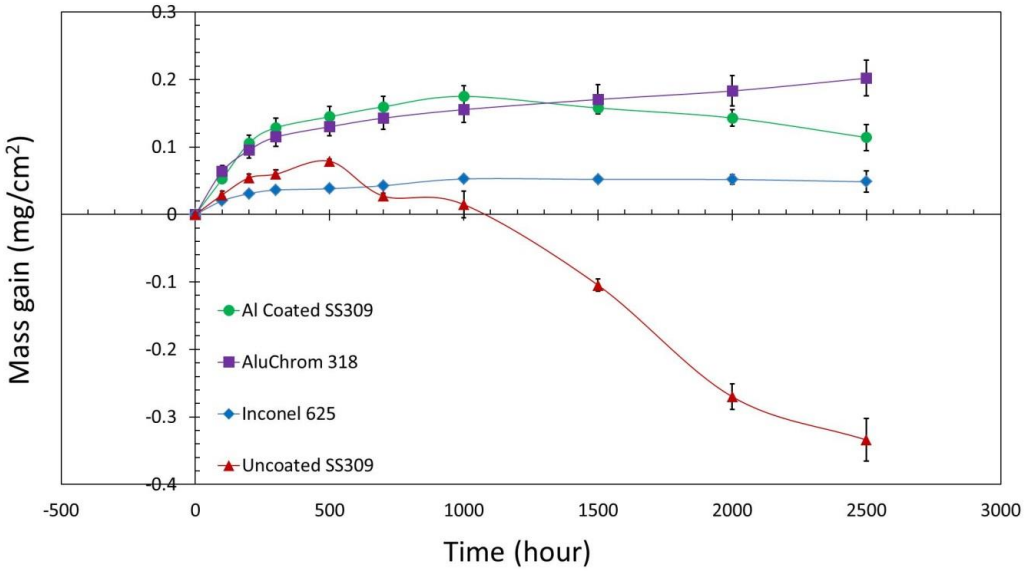

Figure 2. Discontinuous mass measurements for aluminised SS309, AluChrom 318, Inconel 625, and uncoated SS309 in 3 vol% H_2O humidified air at 850 ˚C.

Figure 2 shows the mass gain of the four materials, AluChrom 318, Inconel 625, uncoated SS309, and Al coated SS309, as a function of time. The samples were exposed at 850 ˚C with 6.0 L/min air + 3 vol% H_2O for 2500 hours. Up to 500 hours, the uncoated SS309 substrate showed a parabolic oxidation mechanism with a total mass gain of 0.079 mg/cm^2. However, the substrates appeared to then show a mass loss and suffered from severe scale spallation over 2500 hours. It was observed that after 500 hours a large amount of black powder was detected on the sample holder of the SS309, while the sample holders of other samples remained clean. The serious mass loss noted for uncoated SS309 was due to a combination of spallation of the oxide scale and evaporation of chromium species. This suggested that the oxide layer formed on the SS309 surface was poorly adherent and not durable in simulated SOFC cathode environment. The same mass loss behaviour was also detected from E-Brite by Sachitanand et al. [12], and they attributed the mass loss to the porous structure and bad adherence of oxide scale on the E-Brite surface. On the other hand, the aluminised SS309 showed a high and rapid mass

ISBN 978-3-905592-23-8

gain without spallation. As can be seen, a mass gain of about 0.160 mg/cm^2 was recorded after 1000 hours, which is higher than that of the other Cr-containing steels. This was primarily because of the fast reaction rate between Al and O in the early exposure, accompanied by the formation of an alumina scale. Furthermore, the mass loss from Cr evaporation was minimised due to the presence of the outer alumina scale. Nicolls *et al.* [13] reported that a higher oxidation rate was noticed for alloys with higher Al content at high temperature. However, the aluminised SS309 started to suffer mass loss after 1000 hours exposure due to the exfoliation of the formed alumina scale. The Ni based alloy, Inconel 625, showed a relatively low mass gain of about 0.048 mg/cm^2 after an exposure time of 2500 hours. This low mass gain is made up of a large volatilisation loss and diffusion controlled accumulation, indicating that the oxide scale formed on the surface of Inconel 625 is not protective in humidified atmosphere at high temperature. AluChrom 318 with 3.58% Al content exhibited a mass gain of 0.143 mg/cm^2 which is slightly lower than aluminised SS309 prior to 1000 hours. A total mass gain of 0.202 mg/cm^2 was reached after 2500 hours exposure. Interestingly, all the Al-containing materials showed a relatively higher mass gain rate compared to the chromia-forming alloys (uncoated SS309 and Inconel 625) without Al addition. This was because the protective Al-rich oxide layer that formed effectively protected the steel from high temperature Cr evaporation in SOFC cathode environment.

3.2 Chromium Evaporation

The results of time resolved Cr evaporation tests performed on the investigated steels under isothermal conditions are presented in Figure 3. Figure 4 shows the concentration of the critical elements present on the alloy surface before and after the high temperature oxidation test. A comparison of the four materials revealed that a linear time dependence of the Cr evaporation was obtained from the pure chromia scale formed on the Inconel 625 surface with the highest amount of Cr evaporation (0.06 mg/cm^2), a factor of ten higher than AluChrom 318 and aluminised SS309. Furthermore, it can be seen from Figure 3(c) that the increase of Cr concentration from 13.33 at% (100 hours) to 20.52 at% (1000 hours) indicates a thicker chromia scale is formed on the alloy surface, which is considered to be a detrimental factor for Cr leakage. This is in good agreement with the mass gain results that Inconel 625 has the lowest value of mass gains, as shown in Figure 2, which can be attributed to the highest amount of Cr evaporation among these alloys [11].

A less linear time dependence of Cr evaporation was detected for SS309 with the second largest amount of Cr loss (0.051 mg/cm^2), which slightly decreaseD with exposure time. As shown in Figure 4(a), the SS309 surface contained a relatively high amount of Cr and Mn that result in the formation of (Cr,Mn) spinel as outer scale. Obviously, the (Cr,Mn) spinel layer formed on SS309 shows a better Cr retention ability than the pure Cr_2O_3 formed on Inconel 625 because of the lower Cr partial pressure over the (Cr,Mn) spinel layer compared to pure Cr_2O_3 scale [14]. The Cr diffusion from the oxide/metal interface to the oxide surface is considered as the rate determining step for the Cr evaporation in this case. The evaporated Cr can be rapidly replaced by the fast transportation of Cr via the (Cr,Mn) spinel layer due to the high amount of defects in the spinel layer. It can be speculated that the formed (Cr,Mn) spinel layer may reduce Cr evaporation but does not form a true barrier layer since the Cr evaporated from SS309 still remains at an unacceptable level [10, 14].

www.EFCF.com/Lib
ISBN 978-3-905592-23-8

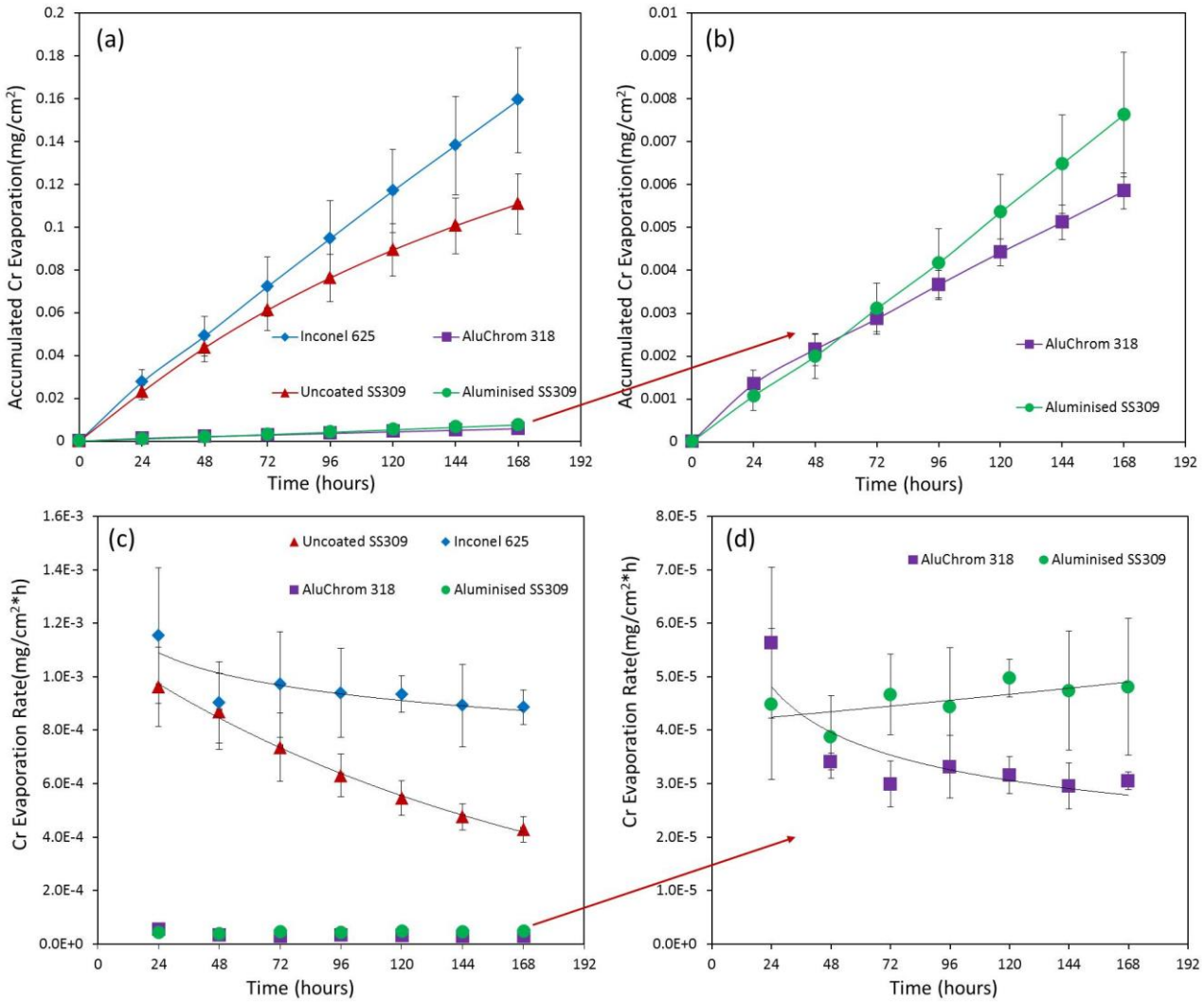

Figure 3. (a-b) Accumulated Cr evaporation for Inconel 625, Uncoated SS309, AluChrom 318 and aluminised SS309 exposed to 3 vol% H_2O humidified air, 850 ˚C for 168 hours; (c-d) Cr evaporation rate as a function of time for Inconel 625, Uncoated SS309, AluChrom 318 and aluminised SS309.

The best Cr retention ability was observed with AluChrom 318 with the lowest amount of Cr evaporation (0.006 mg/cm^2) of all the materials due to the formation of the Al_2O_3 layer acting as a more effective Cr barrier. The formed alumina layer restrains the surface chromium evolution through restraining the ionic mobility of chromium and oxygen throughout the alumina scale. Quadakkers [15] suggested that the growth of a RE (reactive element) doped Al_2O_3 layer on the steel surface is dominated by the inward migration of oxygen through grain boundaries. The grain boundaries can be blocked by trace amounts of reactive elements such as Y, Hf, Zr, thereby preventing the cations such as Cr^{3+} from outward diffusion [15, 16]. In Figure 3(d), the high Cr evaporation rate in the first day of test resulted from the chromium rich oxides formed in the initial stage, leading to the chromium evaporation before eventual development of the continuous Al_2O_3 layer. Furthermore, EDX results suggest that the Cr concentration detected on the AluChrom 318 surface stayed constant (around 2 at%) from 500 hours onwards, indicating that alumina-forming steel could reduce high temperature Cr evaporation in the long term.

ISBN 978-3-905592-23-8

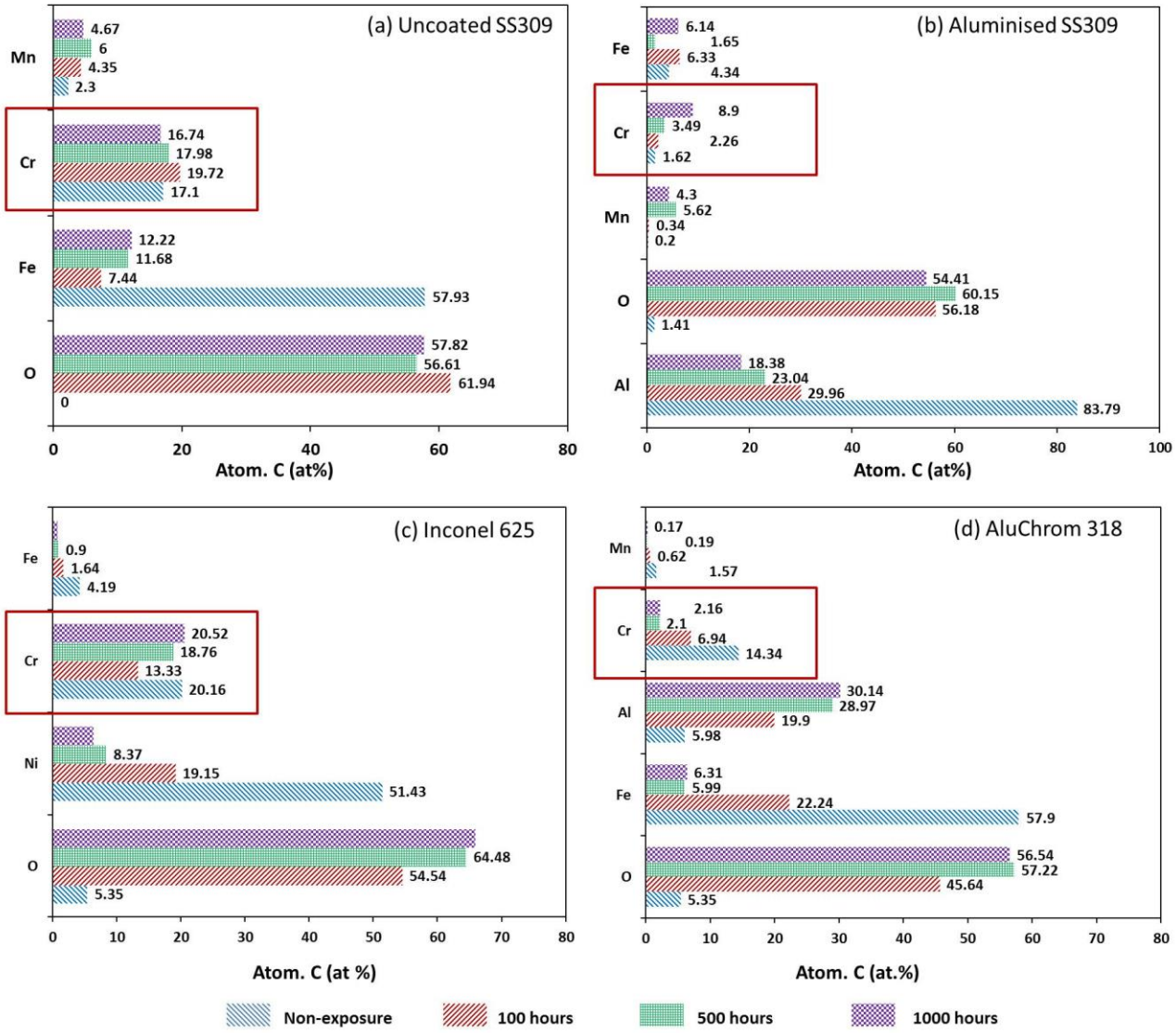

Figure 4. EDX elemental concentration on alloy surface exposed at 850 ˚C for 0, 100, 500 and 1000 hours: (a) uncoated SS309, (b) aluminised SS309, (c) Inconel 625, and (d) AluChrom 318.

The Cr evaporation rate for the aluminised SS309 (0.006 mg/cm^2) was approximate one order of magnitude lower than that for the uncoated SS309 (0.051 mg/cm^2). The measured Cr evaporation of aluminised SS309 was comparable to that of AluChrom 318, indicating the excellent Cr retention ability of alumina scale. The enhanced Cr retention capability for aluminised SS309 is accredited to the presence of the aluminium coating, which significantly reduces the Cr evaporation from the alloy surface due to the formation of a dense and continuous Al_2O_3-rich scale [10, 17]. The rapid oxidation of the aluminium to an outer Al_2O_3 –rich layer acts as chromium barrier which inhibits the outward diffusion of the Cr element during high temperature exposure; thus a significantly reduced Cr evaporation is observed. Nevertheless, the Cr evaporation rate of aluminised SS309 showed a slightly increased trend after 72 hours (Figure 3(d)), and the Cr concentration dramatically increased to 8.9 at% (Figure 4(b)) after 1000 hours of exposure. This phenomenon was caused by spallation of the formed alumina scale and will be discussed later in the SEM section. The Cr evaporation test for all the four materials were repeated three times with good repeatability, which means that the results obtained from the denuder technique are reliable.

www.EFCF.com/Lib
ISBN 978-3-905592-23-8

3.3 Microstructural Investigation

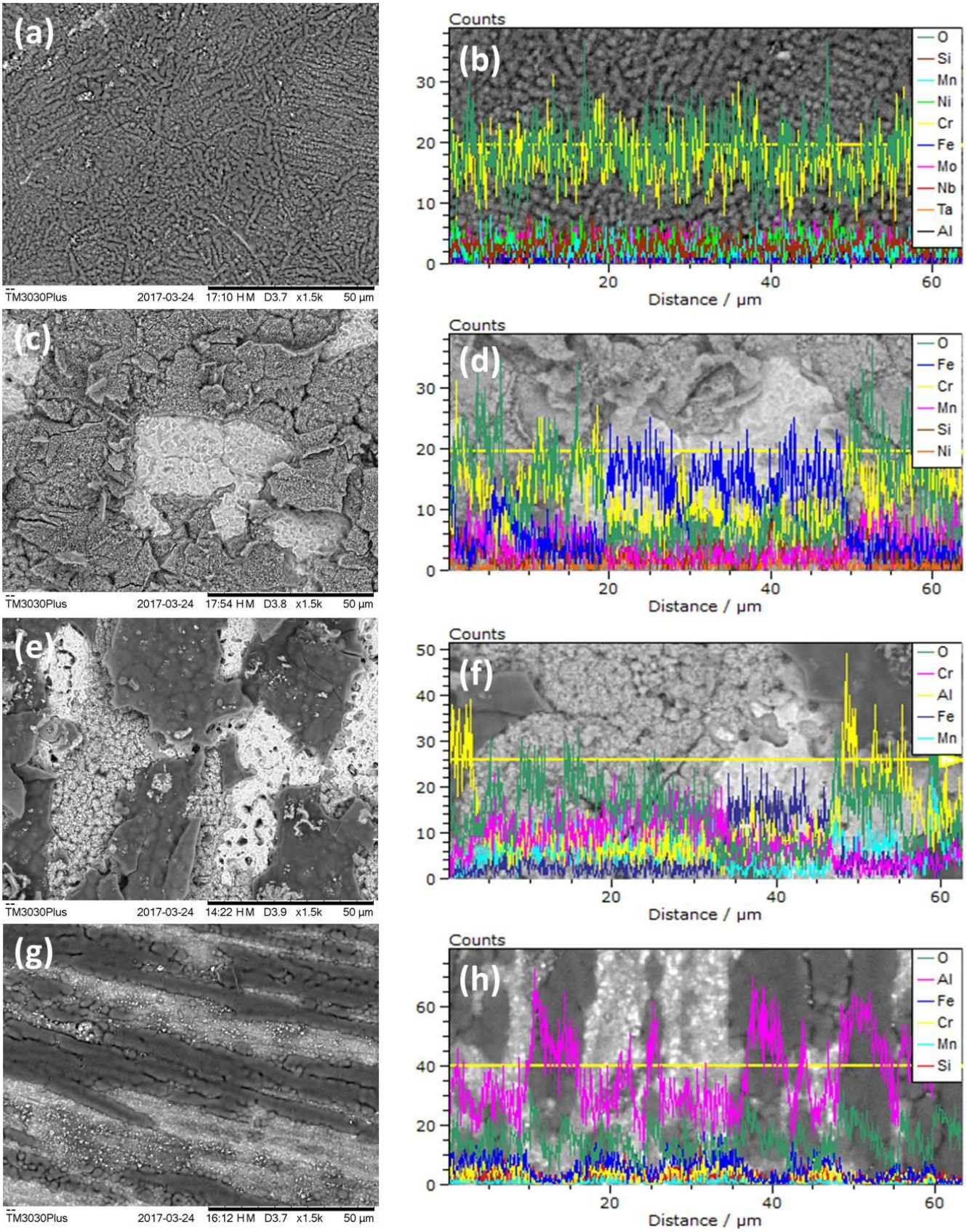

Figure 5. Surface SEM and EDX line scan of the oxide scale of (a and b) Inconel 625, (c and d) SS309, aluminised SS309 and (g and h) AluChrom 318 after oxidation for 1000 hours in air at 800 °C.

ISBN 978-3-905592-23-8

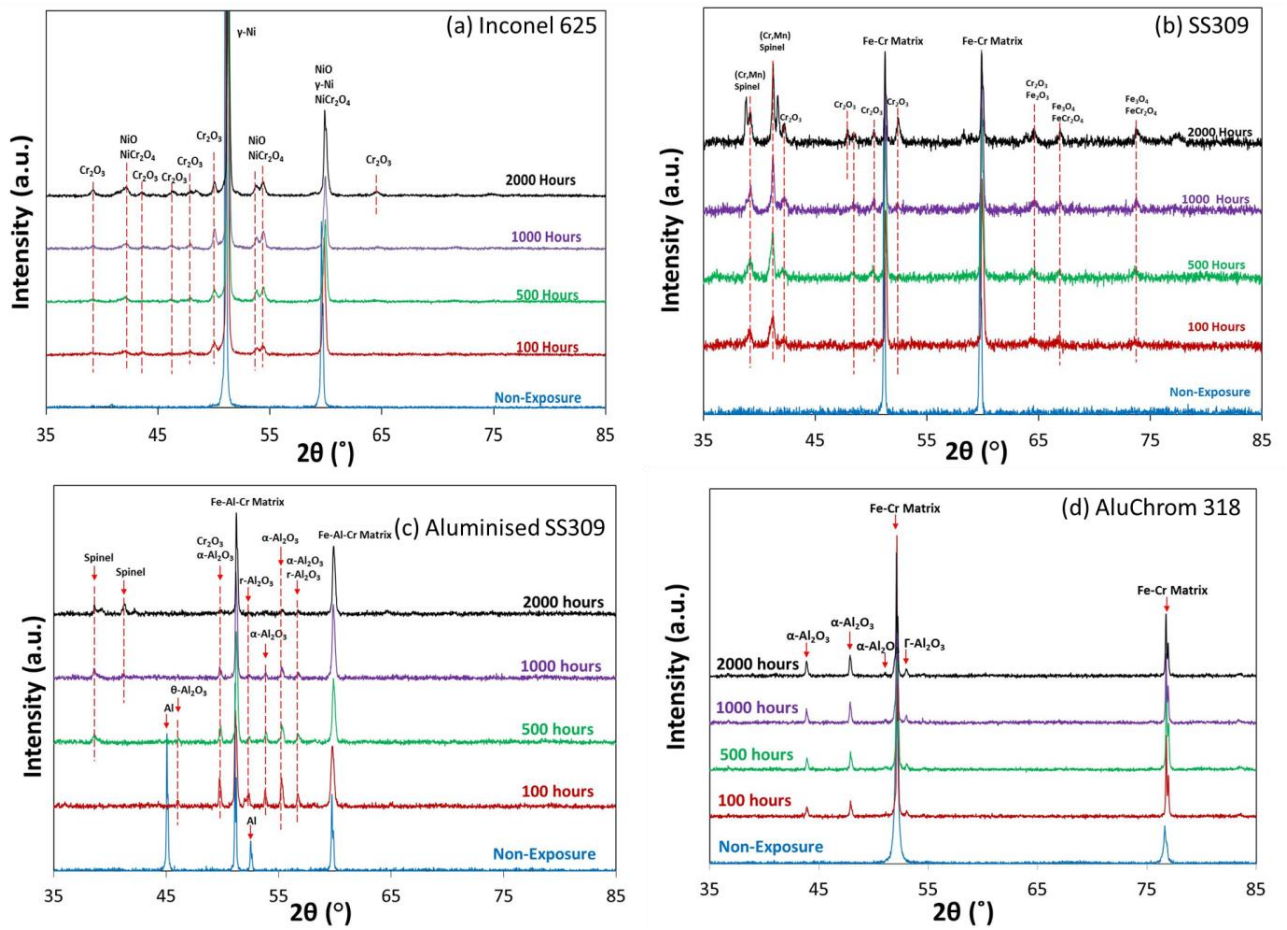

Figure 6. XRD patterns of (a) Inconel 625, (b) SS309, (c) aluminised SS309 and (d) AluChrom 318 exposed at 850 °C for 0 hours, 100 hours, 500 hours, 1000 hours and 2000 hours.

Figure 5 shows the surface SEM and EDX line scans of Inconel 625, SS309, aluminised SS309 and AluChrom 318 after oxidation at 800 °C for 1000 hours. The XRD spectra of Inconel 625, SS309, aluminised SS309 and AluChrom 318 after oxidation at 850 °C for 0 hours, 100 hours, 500 hours, 1000 hours and 2000 hours are shown in Figure 6. For Inconel 625, the upward growth of oxide nodules along the grain boundaries was observed on the surface, and the growth path of oxide granules appeared to have a hexagon of shape, as can be seen from Figure 5(a). Apart from the grain boundaries, it was observed that more oxide grains also grew from the porous surface. Thus, Cr2O3 in the shape of long strips covered the whole alloy surface after 1000 hours of exposure. The XRD spectra of Inconel 625 after 2000 hours of exposure (Figure 6(a)) indicates that the primary oxides formed on the surface were Cr2O3, NiO and NiCr2O4 [18]. It has been reported that spinel oxide (NiCr2O4) may produce at high temperature via the solid solution reaction between Cr2O3 and NiO formed during the initial stage of oxidation [19]. For uncoated alloys, one of the significant factors to offer high temperature oxidation resistance is the formation of the spinel-containing scale for chromium retention [20]. EDX line scan analysis (Figure 5(b)) and EDX composition analysis (Figure 4(c)) taken from the alloy surface indicated the oxide scale formed on the surface after 1000 hours exposure mainly consisted of Cr2O3. However, only low amounts of Ni were detected on the oxide scales, which mean that the formed spinel layer (NiCr2O4) did not have enough surface coverage. Thus, this phenomenon could explain the largest quantity of Cr evaporation from Inconel 625 among the four materials, which also confirms the evaluation from gravimetric measurements (Figure 2).

ISBN 978-3-905592-23-8

For SS309, a cracked oxide layer was formed on the surface after 1000 hours exposure, as shown in Figure 5(c). Furthermore, spallation of the (Cr, Mn)3O4 spinel layer was detected at various positions, exposing the underling chromia to humid air. The small oxide pieces with non-homogeneous size delaminated from the cracked surface, and scattered all around the alloy surface. EDX results (Figure 5(d)) revealed that the surface oxides were composed of high amounts of Cr and Mn with traces of Fe. The formation of the (Cr, Mn) spinel phase was confirmed by XRD after 100 hours exposure. The EDX study (Figure 5(d)) pointed out that the exposed layer beneath the Cr-Mn spinel contained very high amounts of Fe and Ni with traces of Cr. In Figure 4(a), the surface concentration of Cr and Mn showed a decreasing trend with the increasing exposure time while the surface concentration of Fe increased. This is also in good agreement with the XDR results. A clear increase of the Fe-rich oxide peaks and Cr-rich oxide peaks was observed for SS309 with the increase of exposure time from 500 hours to 2000 hours. Results from Grolig et al. [21] are in line with the observation of this study, they also noticed a large amount of spallation on the uncoated AISI 441 exposed at the same conditions as this study for 500 hours. Note that the growth of Laves phases could be dramatically promoted by the addition of niobium content inside the alloy [22]. Grolig et al. [21] stated that the number of Laves phases was not sufficient to bind silica and inhibit subscale silica formation at high temperature, which is generally suggested to induce spallation. In this study, SS309 is categorised as high Si steel (0.75 wt.%) that contains no niobium. Furthermore, the alloy impurity of sulphur is also associated with a greater tendency to scale spallation.
For aluminised SS309, two new XRD peaks which represent aluminium coating were detected for non-exposed aluminised SS309 compared to the uncoated SS309 (Figure 6(c)). The heat treatment in air will prompt the aluminium coating to react with oxygen to form alumina scale on the alloy surface. After high temperature exposure, the aluminised SS309 surface appeared to be covered with alumina oxide scale with small and polygonal crystallite (Mn_2O_3) randomly distributed on the surface (Figure 5(e)). EDX results revealed that the major ingredient of the formed oxide scale mainly consisted of aluminium and oxygen with traces of Cr and Fe (Figure 5(f)). The XRD analysis indicated that the aluminium peaks of the non-exposed sample disappeared after heat treatment. The types of alumina phases formed on the aluminised SS309 surface were confirmed by XRD as a mixture of α-, θ- and γ-alumina, as shown in Figure 6(c). The most surprising finding of this material was that a large amount of spallation was observed for the sample after 1000 hours of exposure. As can be seen from Figure 5(e), a large part of the Al_2O_3-rich oxide scale peeled off from the alloy surface, and Cr-Mn oxide scales and Fe-rich regions were exposed underneath. Similar to XRD analysis, the peak intensity of alumina phases exhibited a continued momentum of decline with the increasing exposure time. Interestingly, the XRD peaks for α-Al_2O_3 almost disappeared for the sample with 2000 hours exposure. It is also worth to notice that the XRD peaks for spinel oxide start to appear on the spectrum after 2000 hours exposure due to the severe delamination of the alumina layer on the aluminised SS309 surface. The XRD results also confirmed that the alumina layer formed on the AluChrom 318 surface was much stronger than that formed on the aluminised SS309 surface. As mentioned above, the formation of a silica layer at the metal/oxide interface is often considered as the most relevant mechanism for oxide spallation on this type of material. EDX analysis showed that the concentration of Si on the aluminised SS309 surface presented an increasing trend from 0 at.% to 1.39 at%. Thus, it can be inferred that the great mass of Si was bound by Laves phases but a small proportion of Si diffused outward, to the oxide/metal interface, leading to spallation of oxide scales [21]. This is also the reason that the high Cr concentration of 8.9 at% was found for aluminised SS309 after 1000 hours exposure (Figure 4(b)). As mentioned above, an increased trend of Cr evaporation rate was noticed for aluminised SS309 after 72 hours

ISBN 978-3-905592-23-8

(Figure 3(d)). This is due to the spallation of Al2O3 scale, leading to the exposure of the Cr-rich oxide layer.

The surface of AluChrom 318 with the exposure time of 1000 hours appeared to be partially covered with a buckled oxide with dark grey colour (Figure 5(g)). No sign of spallation was detected even after 1000 hours of exposure. Similar morphology of this type of oxide scale was also detected by Ge et al. [23] on AluChrom YHf exposed to 3% humid air for 500 hours at 950 °C. EDX results (Figure 5(h)) show that the buckled oxides contain Al and O with a small amount of Mn, indicating that a dense surface scale of Al2O3 had formed [10, 13]. In addition, it can be noticed that the intensity of Al in the non-buckled region was lower than that in the buckled region, which means that the non-buckled region was covered with a relatively thinner alumina scale. After heat treatment, the oxide phases existing in the scale were identified to be of α and γ forms of alumina by XRD analysis, as can be seen in Figure 6(d). It is obvious that α-Al2O3 and γ-Al2O3 forms co-exist after oxidation at 850 °C for 2000 hours and only little γ-Al2O3 can be discovered in the XRD spectrum. Liu et al. [24] state that the γ-Al2O3 phase can be stabilised by water vapour, thereby inhibiting the complete transformation to α-Al2O3. Furthermore, the peak intensity of all alumina phases showed an increasing trend with the increase of exposure time. This reveals that the thickness of the alumina scale kept increasing even after 2000 hours. As mentioned above, the smallest proportion of Cr (2.16 at%) was detected by EDX for AluChrom 318 (Figure 4(d)). The additions of reactive elements such as Zr and Hf inside AluChrom 318 tend to cause micro porosity of the alumina scale. This could be a diffusion path for Cr to grow from the alloy to the oxide surface [25]. After 500 hours oxidation, the gradient of Cr concentration flattened, as indicated by the EDX elemental concentration (Figure 4(d)). This reduction and low level of Cr concentration can be explained by the decrease of alumina scale thickening rate with increasing time.

4. Conclusions

The measurement of Cr evaporation from different alloys by the denuder technique exhibited that the amount of Cr evaporated from alumina-forming steel or aluminised steel are approximate by one order of magnitude lower than those from pure chromia-forming steels. Although the Cr vaporisation level of aluminised SS309 was comparable to that of AluChrom 318 for 168 hours, the Cr retention of AluChrom 318 was confirmed to be better than that of aluminised SS309 in the long term due to the spallation of the Al_2O_3 scale on the aluminised SS309 surface.

5. Acknowledgements

This work was funded by European Union's H2020 Programme through the Fuel Cells and Hydrogen Joint Technology (FCH-JU) under grant agreement No. 700564. The authors would like to gratefully acknowledge the support of our collaborators in the HEATSTACK project.

References

1. Costamagna, P., *The benefit of solid oxide fuel cells with integrated air pre-heater.* Journal of Power Sources, 1997. **69**(1): p. 1-9.
2. Graham, H.C. and H.H. Davis, *Oxidation/Vaporization Kinetics of Cr2O3.* Journal of the American Ceramic Society, 1971. **54**(2): p. 89-93.
3. Hilpert, K., et al., *Chromium vapor species over solid oxide fuel cell interconnect materials and their potential for degradation processes.* Journal of the Electrochemical Society, 1996. **143**(11): p. 3642-3647.

4. Opila, E.J., et al., *Theoretical and Experimental Investigation of the Thermochemistry of CrO2(OH)2(g).* The Journal of Physical Chemistry A, 2007. **111**(10): p. 1971-1980.
5. Ebbinghaus, B.B., *Thermodynamics of gas phase chromium species: The chromium oxides, the chromium oxyhydroxides, and volatility calculations in waste incineration processes.* Combustion and Flame, 1993. **93**(1): p. 119-137.
6. Gindorf, C., L. Singheiser, and K. Hilpert, *Vaporisation of chromia in humid air.* Journal of Physics and Chemistry of Solids, 2005. **66**(2–4): p. 384-387.
7. Jiang, S.P. and X. Chen, *Chromium deposition and poisoning of cathodes of solid oxide fuel cells – A review.* International Journal of Hydrogen Energy, 2014. **39**(1): p. 505-531.
8. Taniguchi, S., et al., *Degradation phenomena in the cathode of a solid oxide fuel cell with an alloy separator.* Journal of Power Sources, 1995. **55**(1): p. 73-79.
9. Brumm, M.W. and H.J. Grabke, *The oxidation behaviour of NiAl-I. Phase transformations in the alumina scale during oxidation of NiAl and NiAl-Cr alloys.* Corrosion Science, 1992. **33**(11): p. 1677-1690.
10. Stanislowski, M., et al., *Chromium vaporization from alumina-forming and aluminized alloys.* Solid State Ionics, 2008. **179**(40): p. 2406-2415.
11. Froitzheim, J., et al., *Investigation of Chromium Volatilization from FeCr Interconnects by a Denuder Technique.* Journal of The Electrochemical Society, 2010. **157**(9): p. B1295.
12. Sachitanand, R., et al., *Evaluation of the oxidation and Cr evaporation properties of selected FeCr alloys used as SOFC interconnects.* International Journal of Hydrogen Energy, 2013. **38**(35): p. 15328-15334.
13. Nicholls, J.R., et al., *8 - Lifetime extension of FeCrAlRE alloys in air. Potential role of enhanced Al reservoir and surface pre-treatment (SMILER)*, in *Novel Approaches to Improving High Temperature Corrosion Resistance*. 2008, Woodhead Publishing. p. 129-160.
14. Stanislowski, M., et al., *Reduction of chromium vaporization from SOFC interconnectors by highly effective coatings.* Journal of Power Sources, 2007. **164**(2): p. 578-589.
15. Quadakkers, W.J., *Growth mechanisms of oxide scales on ODS alloys in the temperature range 1000–1100°C.* Materials and Corrosion, 2004. **41**(12): p. 659-668.
16. Quadakkers, W.J., et al., *Differences in growth mechanisms of oxide scales formed on ODS and conventional wrought alloys.* Oxidation of Metals, 1989. **32**(1): p. 67-88.
17. Chou, Y.-S., J.W. Stevenson, and P. Singh, *Effect of aluminizing of Cr-containing ferritic alloys on the seal strength of a novel high-temperature solid oxide fuel cell sealing glass.* Journal of Power Sources, 2008. **185**(2): p. 1001-1008.
18. Behnamian, Y., et al., *A comparative study of oxide scales grown on stainless steel and nickel-based superalloys in ultra-high temperature supercritical water at 800°C.* Corrosion Science, 2016. **106**: p. 188-207.
19. Chang, K.-H., et al., *Effect of dissolved oxygen content on the oxide structure of Alloy 625 in supercritical water environments at 700°C.* Corrosion Science, 2014. **81**: p. 21-26.
20. Chen, Z., et al., *The effects of temperature and oxygen pressure on the initial oxidation of stainless steel 441.* International Journal of Hydrogen Energy, 2014. **39**(19): p. 10303-10312.
21. Grolig, J.G., J. Froitzheim, and J.E. Svensson, *Coated stainless steel 441 as interconnect material for solid oxide fuel cells: Oxidation performance and chromium evaporation.* Journal of Power Sources, 2014. **248**: p. 1007-1013.

ISBN 978-3-905592-23-8

22. Chiu, Y.-T. and C.-K. Lin, *Effects of Nb and W additions on high-temperature creep properties of ferritic stainless steels for solid oxide fuel cell interconnect.* Journal of Power Sources, 2012. **198**: p. 149-157.
23. Ge, L., et al., *Oxide Scale Morphology and Chromium Evaporation Characteristics of Alloys for Balance of Plant Applications in Solid Oxide Fuel Cells.* Metallurgical and Materials Transactions A, 2013. **44**(1): p. 193-206.
24. Liu, F., et al., *Early stages of the oxidation of a FeCrAlRE alloy (Kanthal AF) at 900°C: A detailed microstructural investigation.* Corrosion Science, 2008. **50**(8): p. 2272-2281.
25. Wessel, E., et al., *Effect of zr addition on the microstructure of the alumina scales on fecraly-alloys.* Scripta Materialia, 2004. **51**(10): p. 987-992.

Remark: Paper runs for publication in EFCF Special Issue Series (www.EFCF.com/LIB, SI EFCF 2018) in Journal 'FUEL CELLS - From Fundamentals to Systems'.